Silicon (2021) 13:4535–4544
https://doi.org/10.1007/s12633-020-00775-w

ORIGINAL PAPER

Reduction of Carbon and Oxygen Impurities in mc-Silicon Ingot Using Molybdenum Gas Shield in Directional Solidification Process

M. Avinash Kumar [1] · M. Srinivasan [1] · P. Ramasamy [1]

Received: 14 July 2020 / Accepted: 12 October 2020 / Published online: 22 October 2020

Abstract

Transient global heat transfer simulations are done to analyse the impact of molybdenum shield on carbon and oxygen impurity formation in mc-silicon grown by Directional Solidification (DS) process. Carbon and oxygen are the two main impurities that have a direct impact on affecting the conversion efficiency of the solar cell. The molybdenum shield effectively guides the argon gas flow within the furnace and carries SiO away from the melt free surface and the incorporation of carbon into the melt from the graphite furnace elements is also reduced. The molybdenum shield within the furnace reduces the incorporation of carbon and oxygen concentration in the ingot thereby enhancing the quality of the ingot. For the ingot grown in the conventional furnace, the higher concentration region of carbon ranges between 2.45×10^{17} atom/cm^3 to 2.25×10^{17} atom/cm^3 and the lower concentration region of carbon ranges between 6.77×10^{16} atom/cm^3 to 8.56×10^{15} atom/cm^3. For the ingot grown with molybdenum shield, the higher concentration region of carbon ranges between 1.06×10^{17} atom/cm^3 to 9.76×10^{16} atom/cm^3 and the lower concentration region of carbon ranges between 4.32×10^{16} atom/cm^3 to 1.61×10^{16} atom/cm^3. Similarly, for the ingot grown in the conventional furnace, the higher concentration region of oxygen ranges between 2.51×10^{17} atom/cm^3 to 2.31×10^{17} atom/cm^3 and the lower concentration region of oxygen ranges between 6.85×10^{16} atom/cm^3 to 7.67×10^{15} atom/cm^3. For the ingot grown with molybdenum shield, the higher concentration region of oxygen ranges between 2.49×10^{17} atom/cm^3 to 2.25×10^{17} atom/cm^3 and the lower concentration region of oxygen ranges between 8.75×10^{16} atom/cm^3 to 9.10×10^{15} atom/cm^3. Simulations are done for the whole DS growth process for the conventional furnace having no molybdenum shield and for the furnaces having molybdenum shield fixed at three different positions. The molybdenum shield incorporation in DS furnace shows a significant impact on uniformity and reduction of carbon, oxygen impurity distribution in the as-grown mc-silicon ingot.

Keywords Impurity transport · Numerical simulation · Solar PV · Silicon · Directional solidification · Conversion efficiency

1 Introduction

Presently, most of the solar cells in the Photovoltaic markets are developed with the help of multi-crystalline silicon. In the solar PV market, almost 60% of the photovoltaic panels are manufactured using mc-silicon cells [1, 2]. The mc-silicon wafers are largely produced from Directional Solidification (DS) process, due to its simple growth mechanism and it has high yield and is highly cost-effective in comparison to Czochralski (CZ) silicon growth. While growing this mc-silicon, there exist many challenges such as optimization of crystal/melt interface, in which the shape of the interface should be planar or slightly convex for uniform growth and reduction of thermal stress to reduce the generation of dislocation [3, 4]. The melt convection also plays a vital role in controlled solidification. The control over grain boundaries and their orientation in a particular direction highly influence the efficiency of the mc-Si cells [5]. The spot cooling and dendritic methods were used in increasing the grain size of the grown crystal. The seed assisted methods were also used to enhance the quality of the crystal by growing them in a particular orientation [6]. The control over temperature profile is more important to achieve uniform crystallization and dislocation-free multi-crystalline silicon. So, these parameters should be kept in control to increase the energy conversion efficiency of mc-silicon solar cells. Out of all the parameters, impurity incorporation and its concentration hugely affect the quality and conversion efficiency of the wafers cut and sliced

✉ M. Srinivasan
srinisastri@gmail.com

[1] SSN Research Centre, SSN College of Engineering, Chennai 603110, India

from the grown ingot [7–9]. Recently, seed assisted casting mono like multi-crystalline silicon gained huge attention among the commercial crystal grower due to its low cost of production and high yield [10]. To avoid impurity incorporation during the growth of mc-silicon some of the crucible cover mechanisms have been used. The variation in impurity formation and a considerable decrease in impurity incorporation in ingot has been observed by introducing crucible covers within the furnace [11, 12]. The non-metallic impurities, particularly carbon and oxygen tend to cause the carrier recombination phenomenon and to improve efficiency, feedstock and grown ingot should contain an extremely low amount of impurities. The precipitation of silicon carbide tends to occur when carbon concentration exceeds its limit of solubility in silicon and it will result in the generation of new grain and causes ohmic shunts that affect the energy conversion efficiency of solar cells. Oxygen precipitation during solidification affects the wafer's mechanical strength and it also acts as gettering sites for impurities [13]. So, it is essential to control the incorporation of carbon and oxygen in an ingot to achieve high-quality ingots having good conversion efficiency. Experimentally, it is difficult to investigate the dynamics of carbon and oxygen transport phenomena and are highly complicated to measure its precision. And so, numerical simulation acts as an extraordinary tool for investigating the impurity distribution and other heat and mass transfer mechanisms within the furnace. In this work, we have introduced a molybdenum shield inside the DS furnace which is fixed at three different positions to investigate and optimize carbon, oxygen impurity formation in a grown ingot.

2 Numerical Model

The numerical simulation has been done using the Finite Volume Method (FVM). Unstructured and structured grids were formed for modified heater geometry. This Finite Volume method is more suitable for solving this unstructured and structured mesh. The furnace geometry adopted in this work is shown in Fig. 1(a) and (b). The geometry is 2D axisymmetric with respect to axisymmetric boundary conditions [14]. The heat transfer phenomena such as convection, conduction, and radiation were solved by generating triangular and quadrangular grids within the geometry. The flow inside the melt is considered to be laminar and the melt is considered as a Newtonian fluid. Argon was treated as an incompressible ideal gas which is maintained within the chamber [15]. The materials with boundary conditions inside the DS furnace are silicon crystal, silicon melt, molybdenum shield, quartz crucible, argon gas, graphite insulation, heater, heat exchanger block, and steel chamber. CGSim simulation software has been used for all heat transfer computations [16–18]. The impurity measurements are done with the chemical model available in the software. The Navier-Strokes equation has been considered for melt flow. In our numerical simulation, the solid-melt interface is considered as no traction boundary or free boundary in which $\vec{\sigma} \cdot \vec{n} = 0$. Silicon nitrate coating has been used to reduce the crucible constraint and for relaxing thermally induced stress in the grown ingot and so the boundary at bottom and sides of an ingot is also considered as free boundary [19]. The computations are done from the starting to the finishing stage of the solidification process. The heat and mass transfer and species transport phenomena within the furnace are governed by the differential equations given below [20, 21].

$$\frac{\partial \rho}{\partial t} + \nabla.\left(\rho \vec{u}\right) = 0 \tag{1}$$

$$\frac{\partial\left(\rho \vec{u}\right)}{\partial t} + \left(\vec{u}.\nabla\right)\rho \vec{u} = -\nabla p + \nabla.\tau + (\rho - \rho_0).\vec{g} \tag{2}$$

$$\frac{\partial\left(\rho C_p T\right)}{\partial t} + \nabla.\left(\rho c_p \vec{u} T\right) = \nabla.\left(\lambda_{eff} \nabla T\right) + S_T \tag{3}$$

$$\frac{\partial(\rho \phi_i)}{\partial t} + \nabla.\left(\rho \vec{u} \phi_i\right) = \nabla.\left(D_{\phi_i eff} \nabla \phi_i\right) + S_{\phi_i} \tag{4}$$

$$\rho = \frac{p_0 m}{R_g T} \tag{5}$$

$$\tau_{ij} = \mu_{eff}\left(\frac{\partial u_i}{\partial xj} + \frac{\partial u_j}{\partial x_i}\right) - \frac{2}{3}\mu_{eff}\delta_{ij}\nabla.\vec{u} \tag{6}$$

Density- ρ, the reference density - ρ_0, the velocity - $\vec{u}$, the stress tensor - τ, the gravity vector - $\vec{g}$, p - pressure, the specific heat - c_p, the temperature - T, the mass fraction - ϕ_i where i is the species, the effective thermal conductivity - ($\lambda_{eff} = \lambda + C_p \frac{\mu_t}{Pr_t}$), the kronecker delta - δ_{ij}, the effective dynamic diffusivity - $D_{\phi,\ eff}$, the reference pressure - p_0, the molecular weight - m, the universal gas constant - $R_g = 8314 \frac{J}{kmol \cdot K}$, the volumetric source of i-th species - $S_{\phi_i} = S^u_{\varphi_i} + \phi_i S^P_{\varphi_i}$, the sum of turbulent and molecular viscosity is given by effective dynamic viscosity - ($\mu_{eff} = \mu_t + \mu_{molecular}$) and the turbulent Prandtl number $Pr_t = 0.9$.

The incompressible flow of fluid and the gas flow is governed by Eqs. (1)–(4) and the density is calculated using special relations.

3 Results and Discussion

A series of transient global heat and mass transfer simulations are done to investigate the effect of molybdenum shield on the distribution of carbon and oxygen impurities in the mc-silicon ingot grown by DS process. Molybdenum shield has been used in present work due to its low thermal conductivity, small

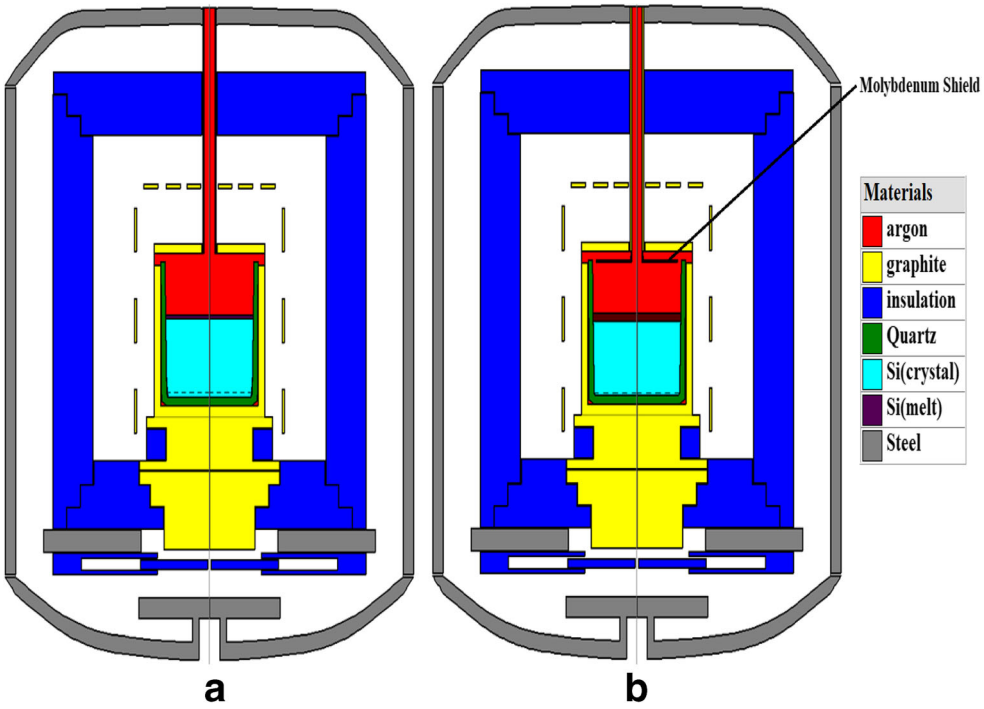

Fig. 1 (**a**) Conventional DS furnace and (**b**) modified DS furnace having molybdenum shield

linear thermal expansion coefficient, and low specific heat capacity [22]. The molybdenum shield also improves concavity of melt/crystal interface thereby reducing the impurity incorporation during the solidification process. We have done a comparative study of impurity distribution in an ingot of size $25 \times 25 \times 15$ cm^3 grown from conventional and modified DS furnace having molybdenum shield fixed at three different positions such as 10 cm (position 1), 5.5 cm (position 2) and 1 cm (position 3) above from the free surface of melt towards top graphite insulation.

3.1 SiO Formation

Oxygen from the quartz crucible gets dissolved into the silicon melt and evaporates from the free surface of melt into argon gas as SiO. The transport phenomena are described in [18] and it is expressed as,

$$Si_{(liquid)} + O_{(liquid)} \leftrightarrow SiO_{(Gas)}$$

The distribution of silicon monoxide above the free surface of the melt is shown in Fig. 2. When molybdenum shield is fixed at the position (1) near the graphite insulation, the SiO concentration tends to get higher above the free surface of the melt and the higher concentration of silicon monoxide was observed near melt and crucible contact region due to the maximum interaction between silicon melt and oxygen from the crucible. SiO vapour is carried away from the free surface of melt by the argon gas towards the top of the furnace and there is a continuous interaction between the SiO and graphite insulation thereby forming a higher concentration of CO above the molybdenum shield. The incorporation of carbon into the growing ingot is minimized with the molybdenum shield by purging maximum of SiO away from the surface of melt by argon and blocking its interaction with the above graphite insulation. When molybdenum shield is in position (2), the concentration of SiO is further minimized above the free surface of the melt and it is carried above the molybdenum shield by argon. The CO formation above the free surface of melt further gets reduced thereby minimizing the incorporation of carbon into the melt. When the molybdenum shield is at the position (3) near the free surface of the melt, the concentration of SiO is extremely low and its maximum volume is carried above the molybdenum shield by argon gas. Thus, the distribution of SiO above the free surface of melt decreases with a decrease in distance between the molybdenum shield and the silicon melt.

3.2 CO Formation

Figure 3 Shows the distribution of carbon monoxide in the furnaces, we see an excess of carbon monoxide above the free surface of melt in the conventional furnace without molybdenum shield. The CO vapour generated from the surrounding graphite units reach the free surface of the melt and the incorporation of carbon and oxygen into the melt is expressed as [18],

$$CO_{(Gas)} \leftrightarrow C_{(Liquid)} + O_{(Liquid)}$$

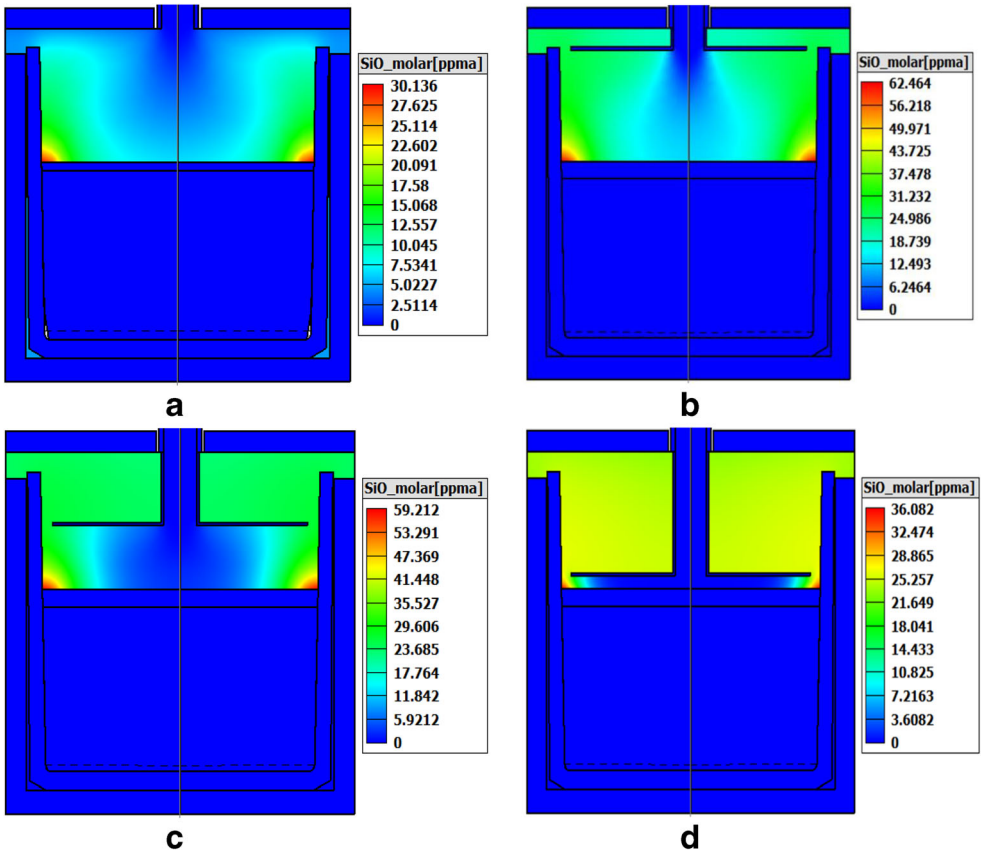

Fig. 2 Distribution of silicon monoxide above the melt free region in (**a**) the conventional furnace and the furnace having molybdenum shield fixed at (**b**) position (1), (**c**) position (2) and (**d**) position (3) within the furnace

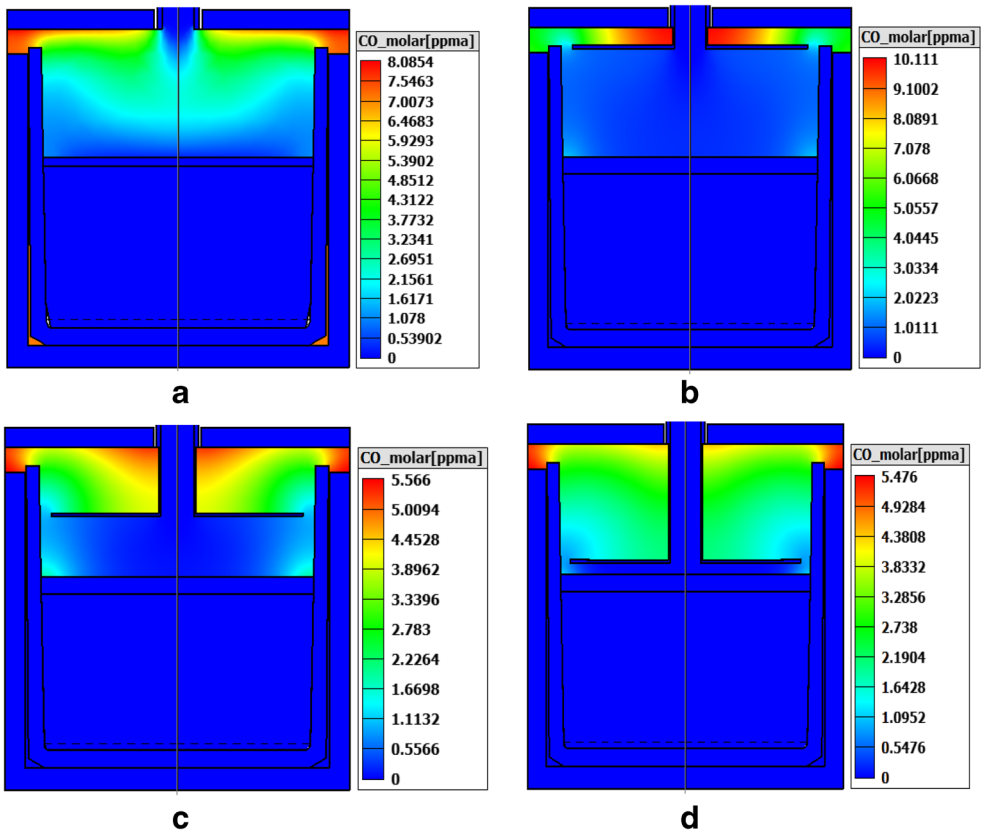

Fig. 3 Distribution of carbon monoxide above the melt free region in (**a**) the conventional furnace and the furnace having molybdenum shield fixed at (**b**) position 1, (**c**) position 2 and (**d**) position 3 within the furnace

Oxygen originated from the crucible reacts with the silicon melt to form SiO and these SiO vapours react with covered graphite elements on the top to form carbon monoxide. In a conventional furnace, the higher concentration of carbon monoxide was observed near the top graphite insulation within the furnace due to the increase in a reaction between SiO from the melt and carbon from the graphite units. The non-homogeneous argon flow also influences the increase in carbon monoxide above the free surface of melt thereby increasing the incorporation of carbon into silicon melt. In the modified furnace having molybdenum shield fixed at position (1), the incoming carbon from the graphite elements has been blocked and the distribution of carbon monoxide above the free surface of the melt is considerably reduced. In the modified furnace, molybdenum shield guides the argon flow within the furnace and SiO vapour is carried away from the free surface of the melt, the higher concentration of carbon monoxide tends to get settled above the molybdenum shield and it minimizes the reaction between SiO and carbon. The argon flow also tends to get regulated with the installation of molybdenum shield thereby restricting carbon impurities. By fixing molybdenum shield at position (2) between graphite insulation and the free surface of the melt, the distance between the shield and the free surface of melt further decreases causing the argon to flow more nearer to the surface and the inhomogeneous carbon monoxide distribution was observed above the molybdenum shield. The SiO vapour from the silicon melt is purged above the shield by argon gas and further minimizes carbon monoxide concentration above the free surface of the melt. When we place it at position (3), the molybdenum shield is fixed very close to the free surface of melt as the distance between them is very small. The argon directly hits the free surface of melt thereby carrying away the maximum amount SiO vapour toward the upper portion of the molybdenum shield and causing extremely low concentration of CO above the free surface of the melt.

3.3 Carbon Concentration

Carbon mainly originates from the graphite units of the furnace and feedstock which leads to the formation of silicon carbide precipitates. Carbon transport is described in [18] and it is expressed as,

$$Si_{(liquid)} + C_{(liquid)} \leftrightarrow SiC_{(solid)}$$

Figure 4 shows the distribution of carbon in the silicon ingot grown in a conventional DS furnace for three different solidification fractions. It shows the gradient increase in the concentration from the bottom towards the top of the growing ingot and attains the maximum value of 2.45×10^{17} atoms/cm^3 after the full growth. Figures 5, 6 and 7 show the distribution of carbon in the silicon ingots grown in a DS furnace

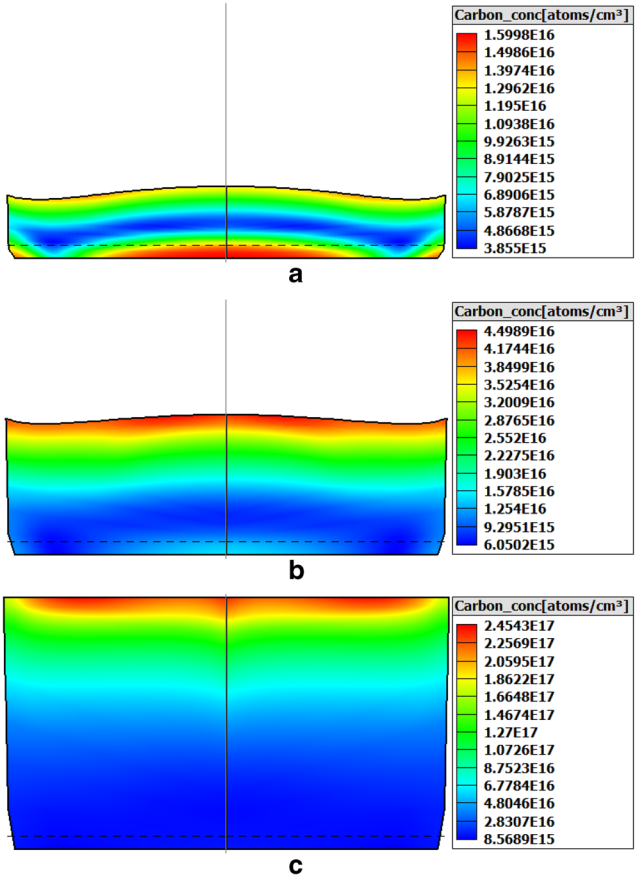

Fig. 4 Carbon concentration for the different solidification fraction at (**a**) 3 h, (**b**) 7 h and (**c**) 30 h for the ingot grown by conventional directional solidification furnace

with the molybdenum shield. The molybdenum shield fixed at three different positions in which position (1) indicates the molybdenum shield fixed near top insulation, position (2) indicates the molybdenum shield fixed at the middle in between top insulation and the free surface of melt and position (3) indicates the molybdenum shield fixed near the free surface of the melt. The melt/crystal interface is w-shaped for the crystals grown at all three positions of molybdenum shield within the furnace. Compared to the conventional furnace, the concavity of melt/crystal interface is improved during solidification of the crystal grown from the furnaces having molybdenum shield. The concentration of carbon is higher at the concave part of the w-shaped interface and the concentration value varies along the radial direction of ingot for each position of the molybdenum shield. During solidification, there is a gradual increase in the concentration of carbon from the bottom to the top of the ingot because of its low segregation coefficient value of 0.7 and so the concentration of carbon is higher on the upper half of the ingot [23]. When the molybdenum shield is installed within the furnace, there is a considerable decrease in the concentration of carbon on the upper half of the ingot. The maximum concentration value

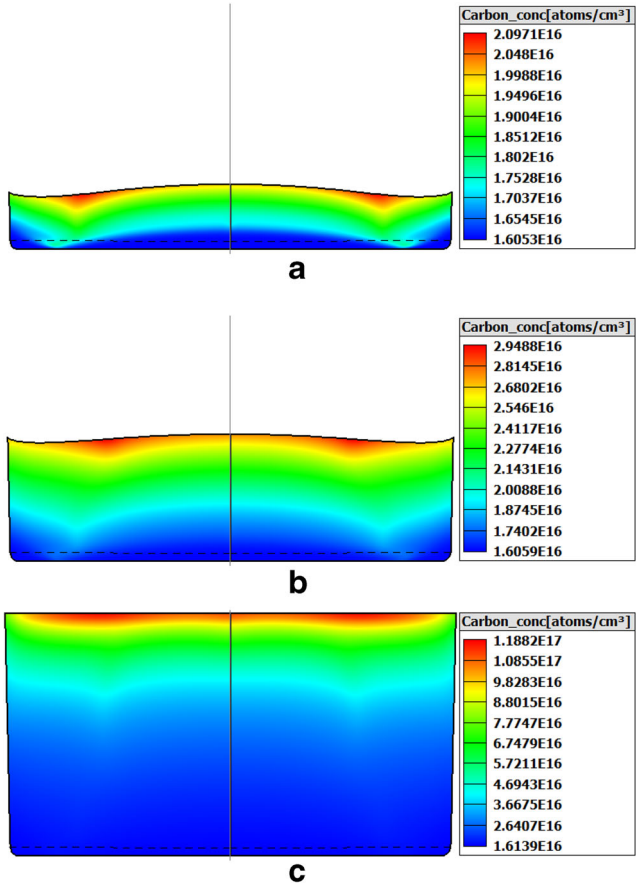

Fig. 5 Carbon concentration for the different solidification fraction at (**a**) 3 h, (**b**) 7 h and (**c**) 30 h for the ingot grown by modified directional solidification furnace having molybdenum shield fixed at the position (1)

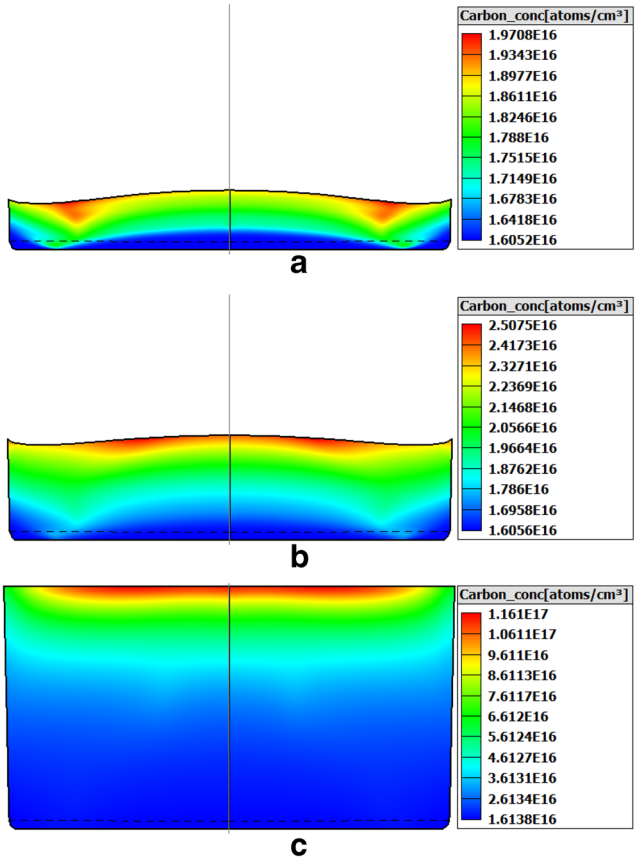

Fig. 6 Carbon concentration for the different solidification fraction at (**a**) 3 h, (**b**) 7 h and (**c**) 30 h for an ingot grown by modified directional solidification furnace having molybdenum shield fixed at the position (2)

decreases from 2.4543×10^{17} atom/cm^3 (without molybdenum shield) to 1.1882×10^{17}atom/cm^3 (top), 1.1610×10^{17}atom/cm^3 (middle) and 1.0666×10^{17} atom/cm^3 (bottom). With a decrease in distance between the molybdenum shield and the free surface of the melt, the concentration of carbon in the ingot also decreases. This is because the amount of SiO was carried away by argon from the free surface of melt increases with the decrease in distance between the molybdenum shield and the free surface of the melt. This phenomenon causes the reduction of SiO generated CO during the solidification process thereby lowering the overall concentration of carbon in the grown ingot. The radial uniformity of carbon distribution in the ingot increases with a decrease in distance between the molybdenum shield and the free surface of the melt. Carbon distribution along the axial direction of the ingots grown from a conventional furnace and modified furnace having molybdenum shield fixed at three different positions is shown in Fig. 8. With an increase in crystal height, the concentration of carbon in the ingots grown in a furnace with molybdenum shield fixed at three different positions has considerably reduced in comparison with the ingot grown from a conventional furnace.

3.4 Oxygen Concentration

As a result of partial melting of quartz crucible, oxygen gets diffused into the silicon melt [18] and it is expressed as,

$$SiO_{2(solid)} \leftrightarrow Si_{(Liquid)} + 2O_{(Liquid)}$$

Figure 9 shows oxygen distribution in the silicon ingot grown in a conventional DS furnace for three different solidification fractions. SiO distribution in the argon atmosphere and the concentration of oxygen in the silicon melt are mainly influenced by melt flow pattern and argon flow [24]. It is observed that the concentration of oxygen in an ingot is higher near the crucible contact region and low on top. The higher concentration values are observed near the bottom and peripheral region of an ingot and the maximum value observed is 2.51×10^{17}atom/cm^3. Due to the higher segregation coefficient value of 1.25, the oxygen concentration is higher at the bottom and there is a gradient decrease towards the top of the ingot. Figures 10, 11 and 12 shows oxygen concentration in an ingot grown with the furnaces having molybdenum shield fixed at three different positions. Normally, the maximum amount of oxygen is diffused into the silicon melt and it is discharged from the free surface of melt through argon carrier

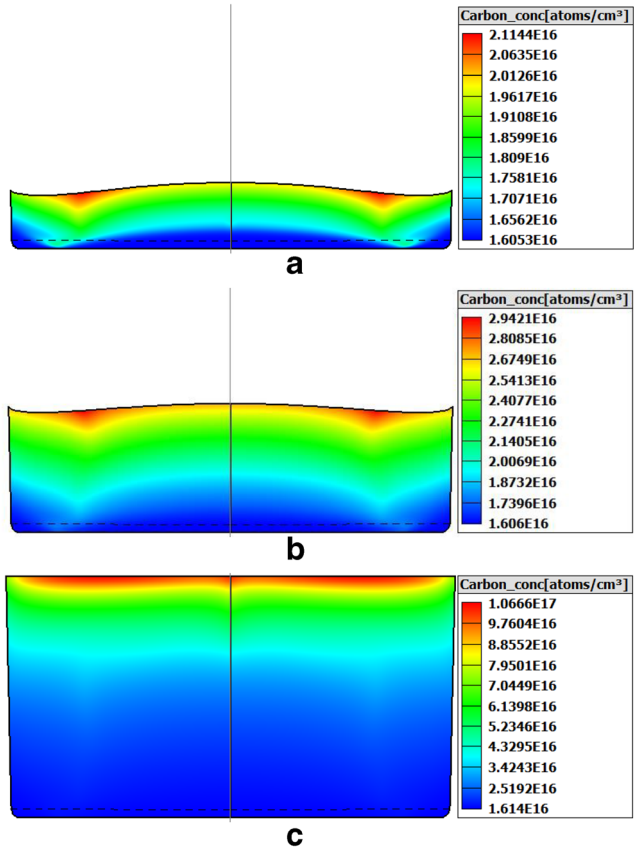

Fig. 7 Carbon concentration for the different solidification fraction at (**a**) 3 h, (**b**) 7 h and (**c**) 30 h for the ingot grown by modified directional solidification furnace having molybdenum shield fixed at the position (3)

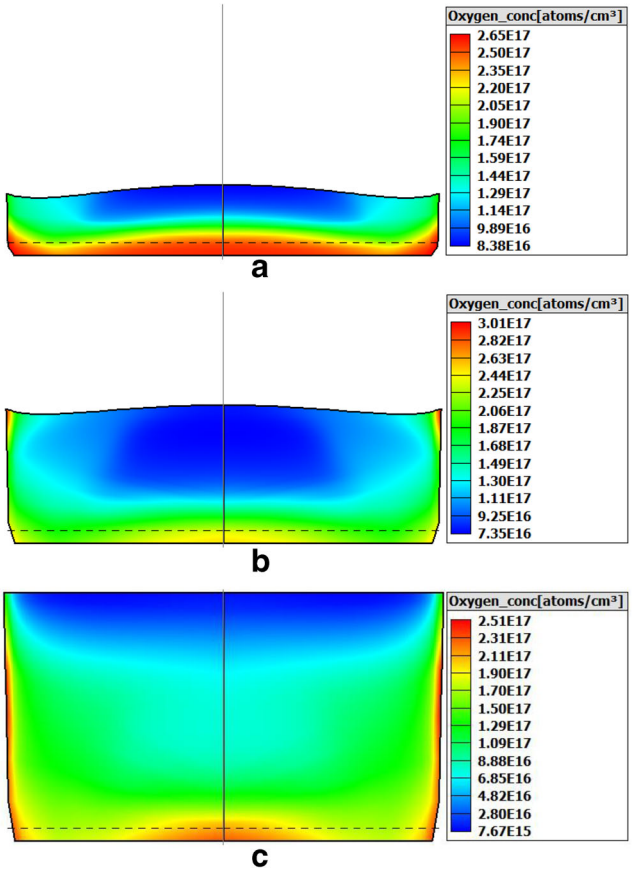

Fig. 9 Oxygen concentration for the different solidification fraction at (**a**) 3 h, (**b**) 7 h and (**c**) 30 h for the ingot grown by conventional directional solidification furnace

gas. So, after the installation of molybdenum shield, oxygen diffused into the silicon melt is effectively purged away from the surface of melt in the form of SiO vapour by argon gas [25]. After the installation of the molybdenum shield, the concentration of oxygen in the middle of the ingot has considerably reduced and the overall concentration of oxygen in the ingot has also reduced. The concentration of oxygen in ingots varies with respect to the distance between the free surface of melt and molybdenum shield. The radial distribution of oxygen in ingots varies for all three positions of molybdenum shield and the variation is observed to be maximum near the peripheral and bottom of an ingot. This variation in the radial distribution of oxygen is due to variation in the transport of SiO from the melt by the argon gas. Oxygen distribution along the axial direction of the ingots grown from a conventional furnace and modified furnace having molybdenum shield fixed at three different positions is shown in Fig. 13. With respect to an increase in height of the crystal, oxygen concentration decreases along the axial direction in the grown ingots. It is observed that the concentration of oxygen is less in the ingots grown with the furnaces having molybdenum shield compared to the ingot grown from the conventional furnace where oxygen concentration is higher at the middle of the ingot.

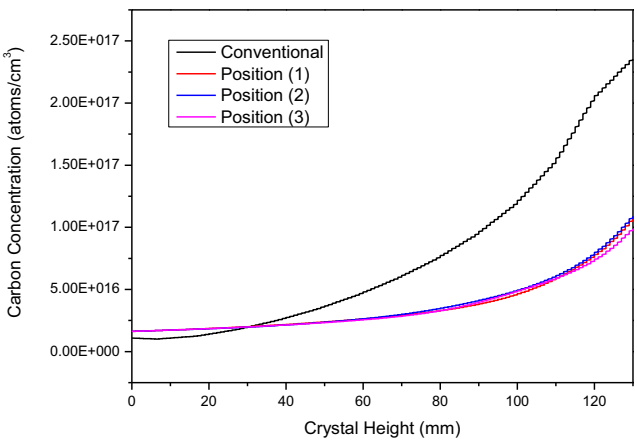

Fig. 8 The distribution of carbon concentration along the axial direction for an ingot grown by conventional DS furnace and for ingots grown by furnace having molybdenum shield fixed at three different positions

The carbon concentration in the ingot decreases with increase in the concentration of CO above the molybdenum shield. As the gap between the molybdenum shield and free surface of melt decreases CO interaction with the melt also decreases thereby decreasing carbon concentration in the

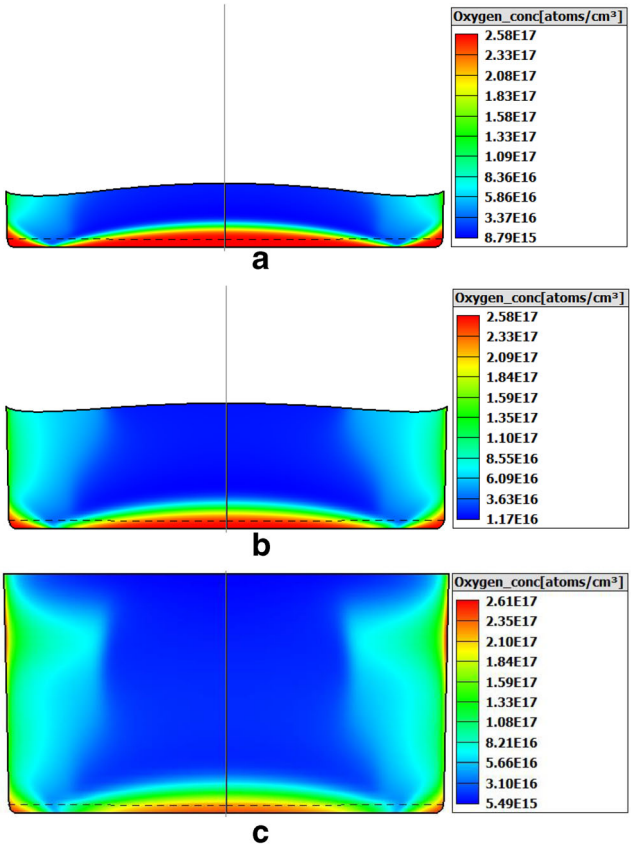

Fig. 10 Oxygen concentration for the different solidification fraction at (**a**) 3 h, (**b**) 7 h and (**c**) 30 h for the ingot grown by modified directional solidification furnace having molybdenum shield fixed at the position (1)

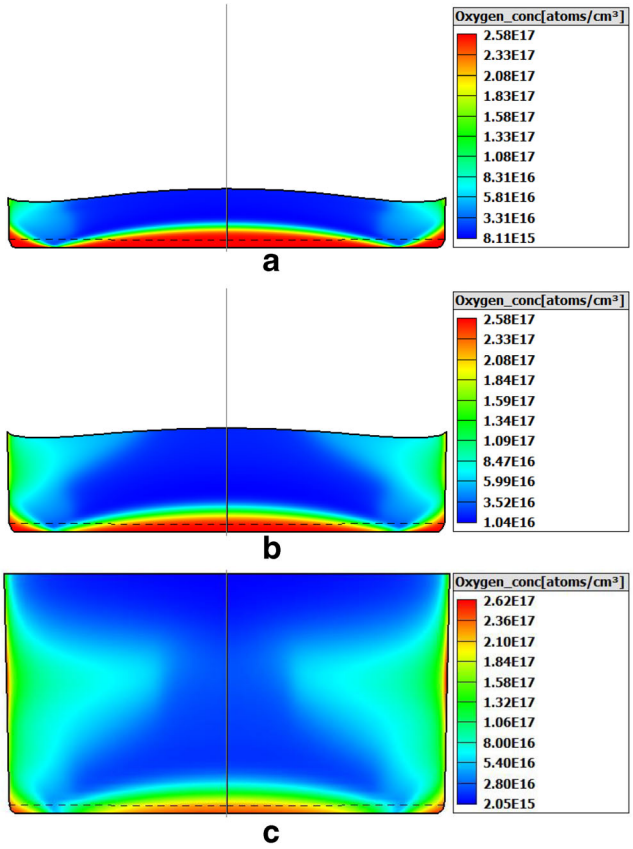

Fig. 11 Oxygen concentration for the different solidification fraction at (**a**) 3 h, (**b**) 7 h and (**c**) 30 h for the ingot grown by modified directional solidification furnace having molybdenum shield fixed at the position (2)

growing ingot. Similarly, the incorporation of oxygen decreases with a decrease in the gap between the molybdenum shield and free surface of melt due to effective purging of SiO by argon gas. There is a variation in radial concentration of oxygen in a growing ingot as the molybdenum shield approaches the free surface due to variation in SiO evacuation by argon gas. When the molybdenum shield is near the free surface of melt at position (3), SiO gas from the free surface of the melt is evacuated effectively by the argon gas and excess of SiO gas from the melt below the free surface tends to remain in the melt during solidification. It results in a slight increase in the concentration of oxygen at the particular area of an ingot where it has an excess amount of SiO in the melt during solidification. The obtained results are similar to the numerical results obtained by Teng et al. [26] in which they used a gas flow guidance device to analyse the impurity transport during the growth of mc-silicon. The impurity distribution within the ingot shows a similar pattern in which carbon concentration is maximum on top of the ingot and decreases towards the bottom and the oxygen concentration in lower on top of the ingot and increases towards the bottom. Thus, the molybdenum shield leads to the reduction of carbon and oxygen impurity concentration in the grown ingots.

4 Conclusion

The non-metallic impurities such as carbon and oxygen impurities are investigated with the modified DS furnace that contains molybdenum shield on the top of the crucible. Due to the installation of molybdenum shield within the furnace, the concavity of the melt/crystal interface improves and it also guides the argon flow inside the furnace. There is an effective flow of argon gas within the furnace in which the evaporated SiO vapour from the free surface of melt and CO produced from the graphite insulation are actively discharged out of the furnace. The argon gas flow near the central region of the free surface of the melt and the argon flow gets stronger with the decrease in distance between the free surface of melt and molybdenum shield. Because of this, argon gas carries away more of the SiO vapour out of the furnace resulting in less formation of CO and reduces its incorporation into the silicon melt out of which it will form SiC particle and oxygen-induced defects that degrade the conversion efficiency. The molybdenum shield blocks the excess of carbon entering into the silicon melt from the surrounding graphite insulation during solidification and it also acts as gas flow guidance that helps in maintaining low carbon atmosphere above the free surface of the melt. Oxygen diffused from the quartz crucible

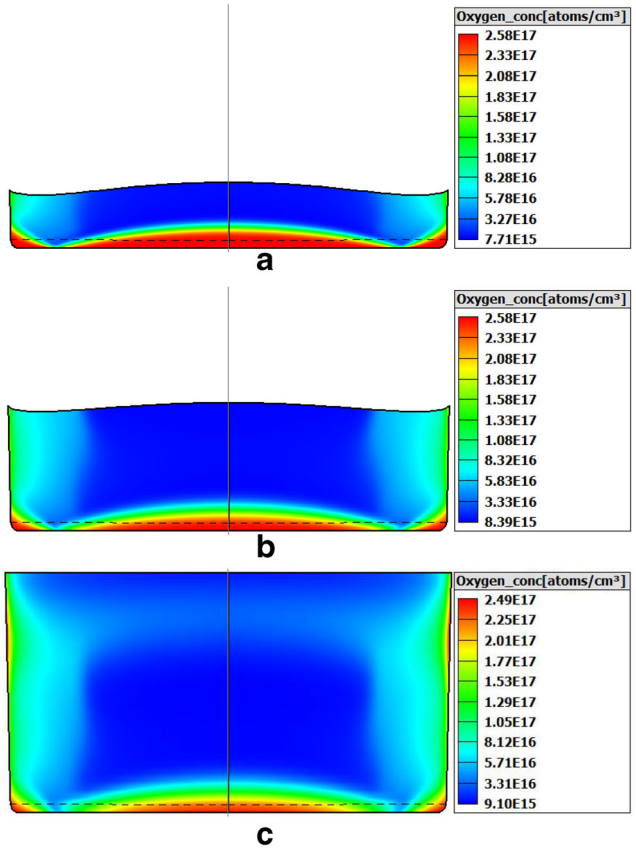

Fig. 12 Oxygen concentration for the different solidification fraction at (**a**) 3 h, (**b**) 7 h and (**c**) 30 h for the ingot grown by modified directional solidification furnace having molybdenum shield fixed at the position (3)

which gets incorporated into the silicon melt is also effectively discharged by the argon gas with the help of molybdenum shield. Thus, the molybdenum shield within the DS furnace acts as an extraordinary tool for minimizing carbon and oxygen impurity concentration in the grown ingots.

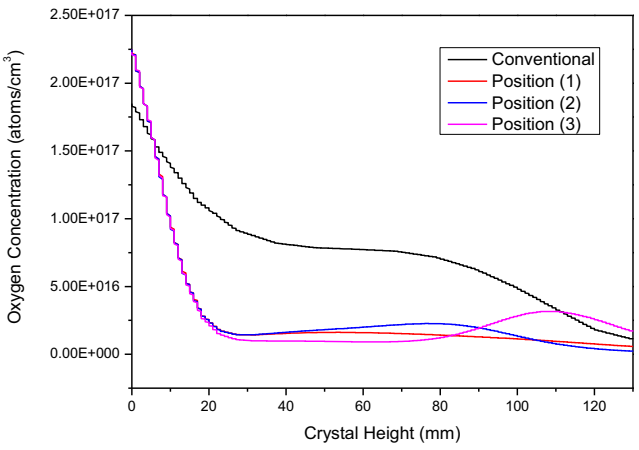

Fig. 13 The distribution of oxygen concentration along the axial direction for an ingot grown by conventional DS furnace and for ingots grown by furnace having molybdenum shield fixed at three different positions

References

1. Wu Z, Zhong G, Zhang Z, Zhou X, Wang Z, Huang X (2015) Optimization of the high-performance multi-crystalline silicon solidification process by insulation partition design using transient global simulations. J Cryst Growth 426:110–116. https://doi.org/10.1016/j.jcrysgro.2015.05.021
2. Xu M, Zheng L (2014) Hui Zhang. J Cryst Growth 385:28–33
3. Chen XJ, Nakano S, Liu LJ, Kakimoto K (2008) Study on thermal stress in a silicon ingot during a unidirectional solidification process. J Cryst Growth 310:4330–4335
4. Jiptner K, Gao B, Harada H, Miyamura Y, Fukuzawa M, Kakimoto K (2014) Takashi Sekiguchi. J Cryst Growth 408:19–24
5. Lin HK, Wu MC, Chen CC, Lan CW (2016) Evolution of grain structures during directional solidification of silicon wafers. J Cryst Growth 439:40–46
6. Lan CW, Yang CF, Lan A, Yang M, Yu A, Hsu HP, Hsu B, Hsu C (2016) Engineering silicon crystals for photovoltaics. Cryst Eng Comm 18:1474–1485
7. Istratov AA, Buonassisi T, Pickett MD, Heuer M, Weber ER (2006) Control of metal impurities in "dirty" multicrystalline silicon for solar cells. Mater Sci Eng B 134:282–286
8. Coletti G (2013) Sensitivity of state-of-the-art and high efficiency crystalline silicon solar cells to metal impurities. Prog Photovoltaics: Res Appl 21:1163–1170
9. Sameshima T, Miyazaki N, Tsuchiya Y, Hashiguchi H, Tachibana T, Kojima T, Ohshita Y, Arafune K, Ogura A (2012) Interaction between Metal Impurities and Small-Angle Grain Boundaries on Recombination Properties in Multicrystalline Silicon for Solar Cells. Appl Phys Express 5:042301
10. Wang P, Cui C, Yang D, Yu X (2020) Seed-Assisted Growth of Cast-Mono Silicon for Photovoltaic Application: Challenges and Strategies. Solar RRL 4:1900486
11. Gao B, Nakano S, Kakimoto K (2011) Effect of crucible cover material on impurities of multicrystalline silicon in a unidirectional solidification furnace. J Cryst Growth 318:255–258
12. Dropka N, Buchovska I, Degenhardt U, Kiessling FM (2020) Influence of impurities from SiC and TiC crucible cover on directionally solidified silicon. J Cryst Growth 542:125692
13. Gao B, Chen XJ, Nakano S, Kakimoto K (2010) Crystal growth of high-purity multicrystalline silicon using a unidirectional solidification furnace for solar cells. J Cryst Growth 312:1572–1576
14. Nakano S, Chen XJ, Gao B, Kakimoto K (2011) Numerical analysis of cooling rate dependence on dislocation density in multicrystalline silicon for solar cells. J Cryst Growth 318:280–282
15. Ding C, Huang M, Zhong G, Liang M, Huang X (2014) A design of crucible susceptor for the seeds preservation during a seeded directional solidification process. J Cryst Growth 387:73–80. https://doi.org/10.1016/j.jcrysgro.2013.08.039
16. Vorob'ev AN, Sid'ko AP, Kalaev VV (2014) Advanced chemical model for analysis of Cz and DS Si-crystal growth. J Cryst Growth 386:226–234
17. Smirnov AD, Kalaev VV (2009) Analysis of impurity transport and deposition processes on the furnace elements during Cz silicon growth. J Cryst Growth 311:829–832
18. Smirnov AD, Kalaev VV (2008) Development of oxygen transport model in Czochralski growth of silicon crystals. J Cryst Growth 310:2970–2976
19. Chen XJ, Nakano S, Liu LJ, Kakimoto K (2008) Study on thermal stress in a silicon ingot during a unidirectional solidification process. J Cryst Growth 310:4330–4335
20. Teng Y-Y, Chen J-C, Lu C-W, Chen C-Y (2010) The carbon distribution in multicrystalline silicon ingots grown using the directional solidification process. J Cryst Growth 312:1282–1290. https://doi.org/10.1016/j.jcrysgro.2009.11.020

21. Hu C, Chen JC, Nguyen THT, Hou ZZ, Chen CH, Huang YH, Yang M (2018). J Cryst Growth 484:70–77
22. Huanga LY, Lee PC, Hsieh CK, Hsub WC, Lan CW (2004) On the hot-zone design of Czochralski silicon growth for photovoltaic applications. J Cryst Growth 261:433–443
23. Liu L, Nakano S, Kakimoto K (2008) Carbon concentration and particle precipitation during directional solidification of multicrystalline silicon for solar cells. J Cryst Growth 310:2192–2197. https://doi.org/10.1016/j.jcrysgro.2007.11.165
24. Li Z, Liu L, Liu X, Zhang Y, Xiong J (2012) Effects of argon flow on melt convection and interface shape in a directional solidification process for an industrial-size solar silicon ingot. J Cryst Growth 360:87–91. https://doi.org/10.1016/j.jcrcysgro.2011.11.053
25. Wenjia S, Chen L, Xiaofang Q, Yang W, Wang J (2019) Numerical analysis and optimization of gas flow and impurity control in directional solidification multi-crystalline. J Cryst Growth 527:125244. https://doi.org/10.1016/j.jcrysgro.2019.125244
26. Teng Y-Y, Chen J-C, Huang B-S, Chang C-H (2014) Numerical simulation of impurity transport under the effect of a gas flow guidance device during the growth of multicrystalline silicon ingots by the directional solidification process. J Cryst Growth 385:1–8. https://doi.org/10.1016/j.jcrysgro.2013.01.040